Chemical Engineering Journal 450 (2022) 137860

Contents lists available at ScienceDirect

Chemical Engineering Journal

journal homepage: www.elsevier.com/locate/cej

Catalyst-free single-step plasma reforming of CH_4 and CO_2 to higher value oxygenates under ambient conditions

Yaolin Wang [a], Yanzhen Chen [a], Jonathan Harding [a], Hongyuan He [a], Annemie Bogaerts [b], Xin Tu [a,*]

[a] Department of Electrical Engineering and Electronics, University of Liverpool, Liverpool L69 3GJ, UK
[b] Research Group PLASMANT, University of Antwerp, Department of Chemistry, Universiteitsplein 1, BE-2610 Wilrijk-Antwerp, Belgium

ARTICLE INFO

Keywords:
Non-thermal plasma
Dry reforming of methane
Biogas utilization
Oxygenates
Methanol synthesis

ABSTRACT

Direct conversion of CH_4 and CO_2 to liquid fuels and chemicals under mild conditions is appealing for biogas conversion and utilization but challenging due to the inert nature of both gases. Herein, we report a promising plasma process for the catalyst-free single-step conversion of CH_4 and CO_2 into higher value oxygenates (i.e., methanol, acetic acid, ethanol, and acetone) at ambient pressure and room temperature using a water-cooled dielectric barrier discharge (DBD) reactor, with methanol being the main liquid product. The distribution of liquid products could be tailored by tuning the discharge power, reaction temperature and residence time. Lower discharge powers (10–15 W) and reaction temperatures (5–20 °C) were favourable for the production of liquid products, achieving the highest methanol selectivity of 43% at 5 °C and 15 W. A higher discharge power and reaction temperature, on the other hand, produced more gaseous products, particularly H_2 (up to 26% selectivity) and CO (up to 33% selectivity). In addition, varying these process parameters (discharge power, reaction temperature and residence time) resulted in a simultaneous change in key discharge properties, such as mean electron energy (E_e), electron density (n_e) and specific energy input (SEI), all of which are essential determiners of plasma chemical reactions. According to the results of artificial neural network (ANN) models, the relative importance of these process parameters and key discharge indicators on reaction performance follows the order: discharge power > reaction temperature > residence time, and SEI > n_e > E_e, respectively. This work provides new insights into the contributions and tuning mechanism of multiple parameters for optimizing the reaction performance (e.g., liquid production) in the plasma gas conversion process.

1. Introduction

Dry reforming of methane (CH_4, DRM) by carbon dioxide (CO_2) for the synthesis of higher value liquid fuels and chemicals has attracted significant interest as both CH_4 and CO_2 are greenhouse gases that contribute to global warming and climate change. This gas-to-liquid (GtL) process is particularly appealing for the conversion and utilization of biogas, which is typically produced by anaerobic digestion (AD) of organic matter such as food, agriculture, and animal waste. Converting biogas (after gas cleaning) to transportable liquids would enable AD viable in locations remote from either the gas or power grids; and thus, potentially allowing access to and use of a broad range of waste. However, direct conversion of CH_4 and CO_2 into oxygenates is not thermodynamically feasible under mild conditions [1]. The traditional thermal catalytic route for liquid synthesis from CH_4 and CO_2 usually consists of two steps: (1) DRM at high temperatures (>700 °C) to produce syngas (a mixture of H_2 and CO); followed by (2) syngas conversion to liquid fuels and chemicals at high pressures. Such a two-step and indirect route for the valorization of CH_4 and CO_2 is energy-intensive, especially given that syngas production from DRM is a highly endothermic process requiring high temperatures and a large energy input. In addition, catalyst deactivation due to coke deposition at high temperatures adds another challenge to finding cost-effective and efficient catalysts for this reaction, thus limiting the use of this process on a commercial scale. Under mild conditions, it is almost impossible to convert these stable and inert molecules (CH_4 and CO_2) directly into liquid fuels and chemicals in a single step using a conventional process (e.g., thermal catalysis).

Non-thermal plasma (NTP) offers a promising and attractive alternative for the activation of CH_4 and CO_2, providing a unique way of

* Corresponding author.
E-mail address: xin.tu@liv.ac.uk (X. Tu).

https://doi.org/10.1016/j.cej.2022.137860
Received 16 May 2022; Received in revised form 25 June 2022; Accepted 28 June 2022
Available online 30 June 2022

enabling thermodynamically unfavorable reactions to take place under ambient conditions [2,3]. This advantage is a result of the unique nonequilibrium character of NTPs, the gas temperature in NTPs can be as low as room temperature or even lower, while the produced electrons are highly energetic with a typical electron temperature of 1–10 eV [4]. This allows them to activate inert molecules with strong chemical bonds, such as CO_2 (5.5 eV) and CH_4 (4.5 eV) and produce a variety of chemically reactive species, including radicals, ions, as well as excited atoms and molecules [5–7]. Moreover, NTP-based processes are highly adaptable, allowing them to be combined with renewable energy sources such as wind and solar power to enable the decentralized electrification of gas conversion and chemical processes. Several types of NTP have been used for the DRM reaction, including glow discharge [8,9], corona discharge [10], microwave (MW) discharge [11], gliding arc discharge [12,13], and dielectric barrier discharge (DBD) [14–18].

So far, research efforts in this area have mainly focused on investigating the plasma DRM reaction for syngas production. For instance, the effects of different reactor configurations, process parameters, packing materials, and catalysts on the performance of plasma DRM for syngas production have been thoroughly studied in terms of the gas conversion, the selectivity and yield of reaction products, as well as the energy efficiency [19–22]. Direct conversion of CH_4 and CO_2 to oxygenates using NTPs, on the other hand, has received less attention. A few groups reported trace amounts of oxygenates as byproducts of plasma-based DRM processes [23–26]. Zou et al., [27] demonstrated that oxygenates could be directly synthesized in the plasma DRM process with a selectivity of 40%. Zhang et al., [28] proved that the distribution of oxygenates could be tailored by using different CH_4/CO_2 molar ratios. Recently, Wang et al., [29] designed a water-electrode DBD reactor for the production of a mixture of oxygenates (e.g., acetic acid, methanol, ethanol, acetone) with a total liquid selectivity of 50–60% at room temperature and ambient pressure. Li et al., [30] found that a smaller discharge gap favored the formation of liquid hydrocarbons (C_{5+}) and acetic acid, whereas a larger gap produced more alcohols (e.g., methanol, ethanol) but with a selectivity of less than 5%. Until now, the single-step and selective synthesis of liquid fuels and chemicals from DRM is still exceptionally challenging. The current state-of-the-art selectivity of total liquid products in this process is 50–60%, reported alongside a relatively low selectivity of individual oxygenates (less than 20%) [29,31]. In addition, for this complex process the intrinsic links among the processing parameters, plasma properties and the reaction performance are largely unclear. For instance, it is unclear how the reaction temperature affects the generation and distribution of liquid products in this process. The quantitative contribution of different process parameters to the production of oxygenates has yet to be investigated. These knowledge gaps limit the potential industrial development of this emerging and promising process.

Herein, we developed a temperature-controlled coaxial DBD reactor for the conversion of CH_4 and CO_2 into oxygenates under ambient conditions with methanol being the major liquid product instead of acetic acid as previously reported [29,32]. Circulating water was used as the ground electrode and for reactor cooling. More importantly, when compared to conventional temperature-controlled DBD plasma reactors and water-electrode DBD reactors, the reaction temperature of this system can be controlled between 5 and 65 °C, thus allowing us to understand the low temperature performance of this promising plasma process which has not been explored before [33]. The influence of various process parameters, such as the CO_2/CH_4 molar ratio, discharge power, reaction temperature, and residence time on the reaction performance of this plasma-based GtL process has been examined. Electrical diagnostics were carried out to determine the mean electron energy (E_e) and mean electron density (n_e) from the electrical signals under various operating conditions. Additionally, plasma spectroscopic diagnostics have been used to investigate the generation of chemically reactive species (e.g., CH, CO, H, and OH) as well as the change of deexcitation channels. Moreover, the relative importance of discharge power, reaction temperature, and residence time in this process was investigated by developing an artificial neural network (ANN) model with a single hidden layer and evaluating the coupling effects of these three parameters on the plasma process. The relationships among the process parameters, the key discharge indicators (i.e., E_e, n_e, and SEI) and the reaction performance have been examined. Furthermore, the optimized ANN models reveal the most advantages and optimal process parameters for the production of target oxygenates in this plasma-based GtL process.

2. Experimental

2.1. Experimental setup

As shown in Fig. 1, the experiments were carried out in a temperature-controlled unconventional coaxial DBD reactor with circulating water as the ground electrode and reactor cooling. Cooling water was circulated between two concentric quartz tubes (50 mm and 14 mm in diameter for the outer and inner tubes, respectively), with the inner quartz tube also acting as a dielectric material for the DBD reactor. A stainless-steel rod with a diameter of 6 mm was used as the high voltage electrode and placed in the axis of the inner quartz tube. In contrast to previous studies [29,32], the reaction temperature of the process in this reactor can be controlled between 5 and 65 °C by the cooling water via a cooling circulation bath (Grant LT Ecocool 150), allowing us to investigate how different low reaction temperatures (5–65 °C) affect the performance of this process for the first time. This reactor is also distinct from conventional temperature-controlled DBD reactors which are typically heated in a tube furnace to higher temperatures (150–500 °C). The length of the discharge region was fixed at 50 mm with a discharge gap of 2 mm, and the discharge volume was about 2.5 mL. A cooling trap was placed at the exit of the DBD reactor to condense liquid products. The gas flow rate was measured before and after the plasma reaction using a soap-film flowmeter. For this study, the DBD reactor was connected to an AC high voltage power supply with a peak voltage of up to 30 kV and a fixed frequency of 9.2 kHz. The applied voltage of the DBD was measured by a high-voltage probe (TESTEC, HVP-15HF), while the current was recorded by a current monitor (Bergoz, CT-E0.5). To measure the charge formed in the DBD, an external capacitor (0.47 μF) was connected between the ground electrode and the ground. All of the electrical signals were sampled by a four-channel digital oscilloscope (Tektronix, MDO3024). The discharge power was calculated using the area of the Lissajous figure. A homemade control software was developed to monitor the discharge power of the DBD in real-time. A fiber optical thermometer (Omega, FOB102) was used to measure the gas temperature in the discharge zone, with the end of the fiber placed in the center of the discharge area (Figure S1a). The gas products were analyzed by gas chromatography (Agilent 7820A) equipped with a flame ionization detector (FID) and a thermal conductivity detector (TCD). A molecular sieve 5A (60–80 mesh) column (HP-MOLESIEVE) was used to separate H_2 and CO, while an HP-PLOT/Q column was used to measure CO_2, CH_4, and C_2-C_4 hydrocarbons. The liquid products were analyzed qualitatively with a gas chromatography-mass spectrometer (GC–MS, Agilent GC 7820A, and Agilent MSD 5977E) and quantitatively with a gas chromatograph (Agilent 7820A) equipped with an FID with a DB-WAX column. Note that no C_{5+} hydrocarbons were detected in this work. Sampling and measurements of the gaseous products began after running the reaction for 4.5 h, and the sampling time of liquid products lasted 6 h. Each measurement was repeated three times to ensure that the measurement error was less than 5%.

Time-averaged optical imaging was performed by an intensified charge-coupled device (ICCD) camera (ANDOR iStar 334 T) attached to a macro lens (Sigma Macro 105 mm F2.8 EX DG) with an exposure time of 50 ms to observe the plasma discharge behavior. The optical emission spectroscopic (OES) diagnostics of the plasma were performed using an optical fiber connected to a Princeton Instruments ICCD spectrometer (Model 320 PI) with a focal length of 320 nm. A 600 g/mm grating was

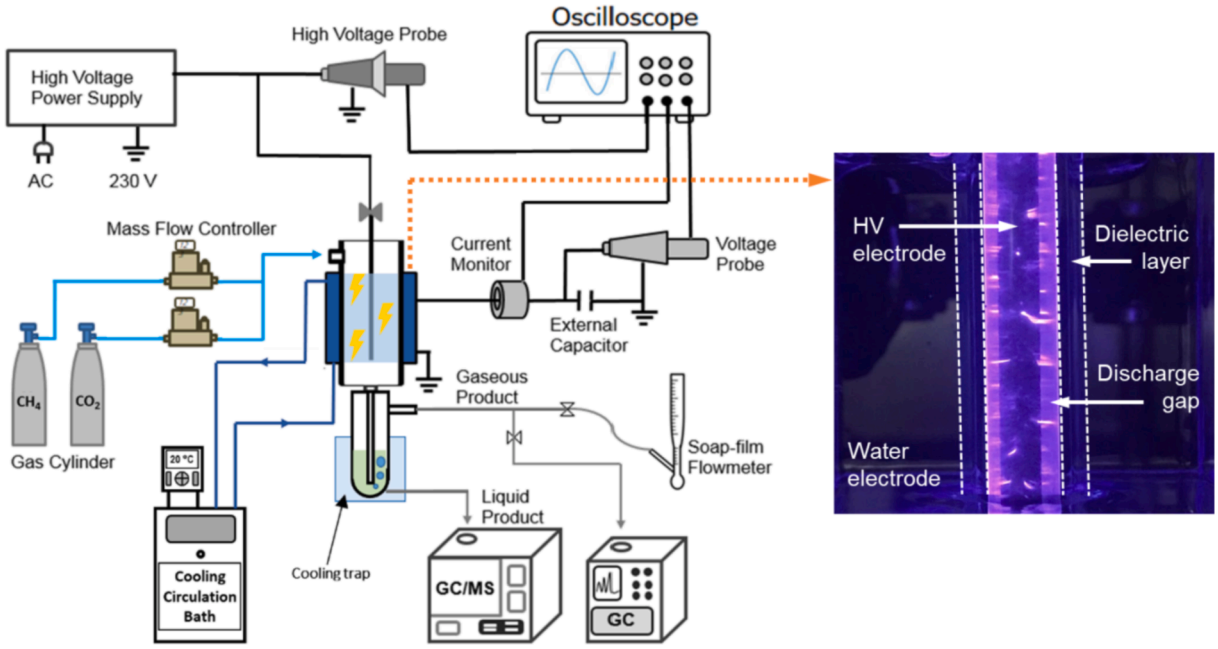

Fig. 1. Schematic diagram of the temperature-controlled water-cooled DBD system and a zoomed-in photo of the DBD reactor with the plasma turned on.

used to record spectra with an exposure time of 0.5 s in the wavelength range of 200–900 nm (Figure S1b).

The gas conversions (X), selectivity (S) of the products, and specific energy input (SEI) are defined as follows:

The conversion of CH_4 and CO_2 is defined as:

$$X_{CH_4}(\%) = \frac{\text{moles of } CH_4 \text{ converted}}{\text{moles of initial } CH_4} \times 100 \quad (1)$$

$$X_{CO_2}(\%) = \frac{\text{moles of } CO_2 \text{ converted}}{\text{moles of initial } CO_2} \times 100 \quad (2)$$

The selectivity of gaseous products is calculated as:

$$S_{H_2}(\%) = \frac{\text{moles of } H_2 \text{ produced}}{2 \times \text{moles of } CH_4 \text{ converted}} \times 100 \quad (3)$$

$$S_{CO}(\%) = \frac{\text{moles of CO produced}}{\text{moles of } CH_4 \text{ converted} + \text{moles of } CO_2 \text{ converted}} \times 100 \quad (4)$$

$$S_{C_xH_y}(\%) = \frac{\text{carbon number of } C_xH_y \times \text{moles of } C_xH_y \text{ produced}}{\text{moles of } CH_4 \text{ converted} + \text{moles of } CO_2 \text{ converted}} \times 100 \quad (5)$$

$$S_{\text{total gaseous products}} = S_{H_2} + S_{CO} + S_{C_xH_y} \quad (6)$$

The selectivity of the total liquid products is calculated as [29]:

$$S_{\text{total liquid products}} = 100\% - \left(S_{CO} + S_{C_xH_y}\right) - \text{ca.10\% carbon deposition} \quad (7)$$

The following experiment was performed to estimate the amount of carbon deposition during the plasma DRM reaction in Eq. (7). Following the plasma DRM reaction under selected operating conditions (e.g., higher discharge power), the DBD reactor was heated in pure O_2 (30 mL/min) at 800 °C to oxidize carbon deposited on the reactor wall and high voltage electrode. The formed gas product was measured using GC. Note that only CO_2 was detected. Carbon deposition was estimated to have a selectivity of less than 10%.

The selectivity of the $C_xH_yO_z$ products is calculated as:

$$S_{C_xH_yO_z} = \text{carbon of } C_xH_yO_z \text{ (mol \%) in the liquid product} \times S_{\text{total liquid products}} \quad (8)$$

where x and y represent the numbers of C and H atoms in each product.

The specific energy input (SEI) for each molecule is defined as:

$$\text{SEI (eV/molecule)} = \frac{\text{discharge power (kW)}}{\text{flow rate (L/min)}} \times 60 \text{ (s/min)} \times \frac{6.24 \times 10^{21} \text{ (eV/kJ)} \times \text{molecule density (L/mol)}}{6.02 \times 10^{23} \text{ (molecule/mol)}}$$

The energy efficiency for the conversion of reactants or produced products is defined as:

$$\text{Energy efficiency (mol/kWh)} = \frac{\text{moles of converted reactants (or produced products) (mol/h)}}{\text{discharge power (kW)}} \quad (10)$$

2.2. Description of the ANN model

ANN, a traditional supervised learning algorithm, was used to predict this complex plasma-driven DRM process under different conditions [34,35]. Two typical single-layer ANN models (ANN_1 and ANN_2) were developed to predict the plasma DRM process and gain new insight into the relative importance of different process parameters (in ANN_1) and key discharge indicators (in ANN_2) on the reaction performance (including "conversion & selectivity" and "energy efficiency"). Both ANN models were implemented using the TensorFlow module, and the

logical structure of the ANN_1 and ANN_2 models is illustrated in Figures S2a and S3a, respectively. A Min-Max normalization was used to pre-treat all data sets, including the input parameters and the predicted results. To solve the nonlinear problem, the Sigmoid Function was chosen as the activation function for both ANN models. To evaluate the performance of these two ANN models, the mean squared error (MSE) was defined as the mean difference between the experimental data (R_i) and the predicted results (P_i),

$$MSE = \frac{1}{n}\sum_{i=1}^{n}(P_i - R_i)^2 \quad (11)$$

During the training process, 13 neurons were selected for the hidden layer when the ANN_1 and ANN_2 models reached a minimum MSE of 0.0046 and 0.0057, respectively. Additionally, 20% of the experimental data were chosen randomly as a test set to validate the ANN models, and the regression plots for comparing experimental and prediction results are presented in Figures S2b, S2c and S3c, respectively. Garson's algorithm was used to calculated the relative importance of variables [36–38].

Two non-dimensional indices, I_1 and I_2 ($0 < I_1, I_2$ less than 1), were introduced to comprehensively evaluate the effectiveness of the plasma DRM process [34,39]. I_1 and I_2 are defined as the product of the normalized (N) conversion of CO_2 and CH_4 or the selectivity of major products, respectively, in combination with the corresponding energy efficiency, based on the global desirability functions. These indicators can be used to optimize the process, resulting in improved performance and increased energy efficiency.

$$I_1 = N\ (\text{gas conversion}) \times N\ (\text{energy efficiency}) \quad (12)$$

$$I_2 = N\ (\text{product selectivity}) \times N\ (\text{energy efficiency}) \quad (13)$$

3. Results

3.1. Effect of CO_2/CH_4 molar ratio

Fig. 2 shows the effect of the CO_2/CH_4 molar ratio on the conversion of CH_4 and CO_2, as well as product selectivity. When the CO_2/CH_4 ratio was changed from 3:1 to 1:3, the CH_4 conversion decreased gradually from 38% to 22%, while the CO_2 conversion reached a maximum of 29% at a CO_2/CH_4 molar ratio of 1:1. The effect of the CO_2/CH_4 molar ratio on the selectivity of total liquid products followed the same tendency as the CO_2 conversion. The main gas products included CO, H_2, and C_2H_6; while methanol, ethanol, acetic acid, and acetone were identified as the main liquid products. Interestingly, methanol has three times selectivity of the other liquid products. Notably, the selectivity of liquid products reached a maximum of 60% at a CO_2/CH_4 molar ratio of 1:1. As both CH_3 and OH radicals are crucial for methanol formation, the highest methanol selectivity of 39% was also achieved at the optimal CO_2/CH_4 molar ratio of 1:1. In addition, a CO_2/CH_4 molar ratio of 1:3 enhanced the production of gaseous products (55% selectivity), particularly light hydrocarbons (C_2-C_4), indicating that the presence of excess CH_4 molecules enhanced the formation of the C–C bond in the plasma. Meanwhile, the energy efficiencies for the conversion of CO_2 and CH_4 exhibited opposite trends as the CO_2/CH_4 ratio changed, and the energy efficiency of methanol synthesis reached the maximum of 0.83 mol/kWh (Figure S4a). As a result of these findings, we conducted the following experiments with a CO_2/CH_4 molar ratio of 1:1.

3.2. Effect of discharge power

The discharge power is a crucial operating parameter for the plasma dry reforming process (Fig. 3a-d). By increasing the discharge power, the conversion of CH_4 and CO_2 increased from 24% to 42% and from 24% to 35%, respectively. In this study, a higher discharge power generated more gaseous products and fewer oxygenates. The selectivity of CO and H_2 was increased by 13% when raising the discharge power, while the selectivity of light hydrocarbons (C_2-C_4) remained nearly unchanged. In addition, the selectivity of CH_3OH increased initially with increasing discharge power, reaching a peak of 39% at 15 W, and then slightly decreased when further varying the discharge power from 20 to 40 W. This was consistent with the overall trend in energy efficiency. Methanol production also achieved the highest energy efficiency at 15 W (Figure S4b). Furthermore, the selectivity of acetic acid decreased rapidly from 24% to 0% when increasing the discharge power.

The electrical signals (Figures S5a, S5b) and the Q-U Lissajous figures (Fig. 3e) were collected to better understand the influence of discharge power on the reaction performance of the plasma DRM reaction. The amount of transferred charge (Q_{trans}) increased in one cycle of the applied voltage as the discharge power increased (Fig. 3f), indicating that a higher discharge power produces more energetic electrons. This finding can be supported by the increased intensity and quantity of discharge pulses in the current signals at a higher power (Figure S5b), revealing that more intense streamer filaments were formed across the discharge gap. When the discharge power was doubled from 10 to 20 W, the effective capacitance (C_{eff}) increased by 10 pF during the plasma-on period, then remained stable at around 53 pF when the power was over 20 W (Fig. 3g). Since C_{eff} is proportional to the spatial distribution of the

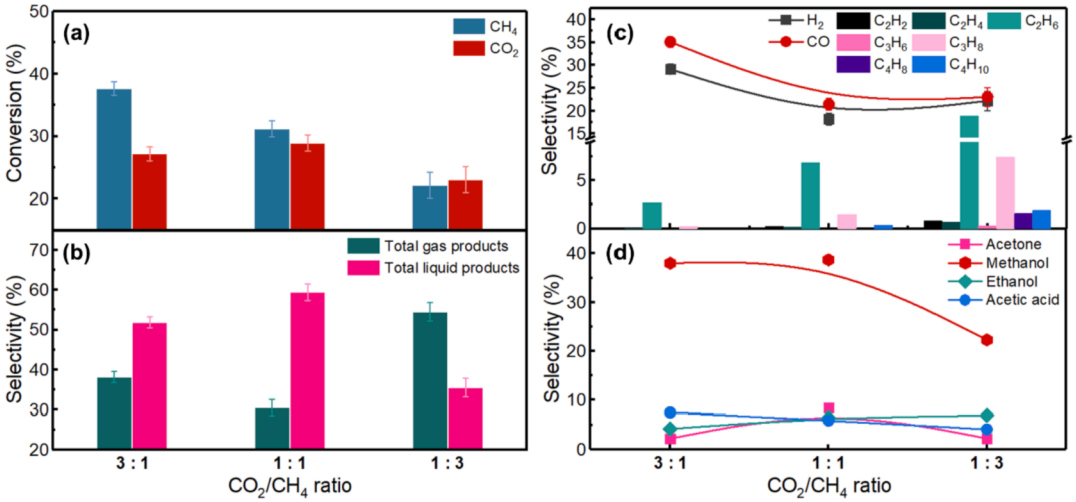

Fig. 2. Effect of different CO_2/CH_4 molar ratios on (a) the conversion and (b-d) the distribution of products (flow rate: 40 mL/min; discharge power: 15 W; reaction temperature: 20 °C).

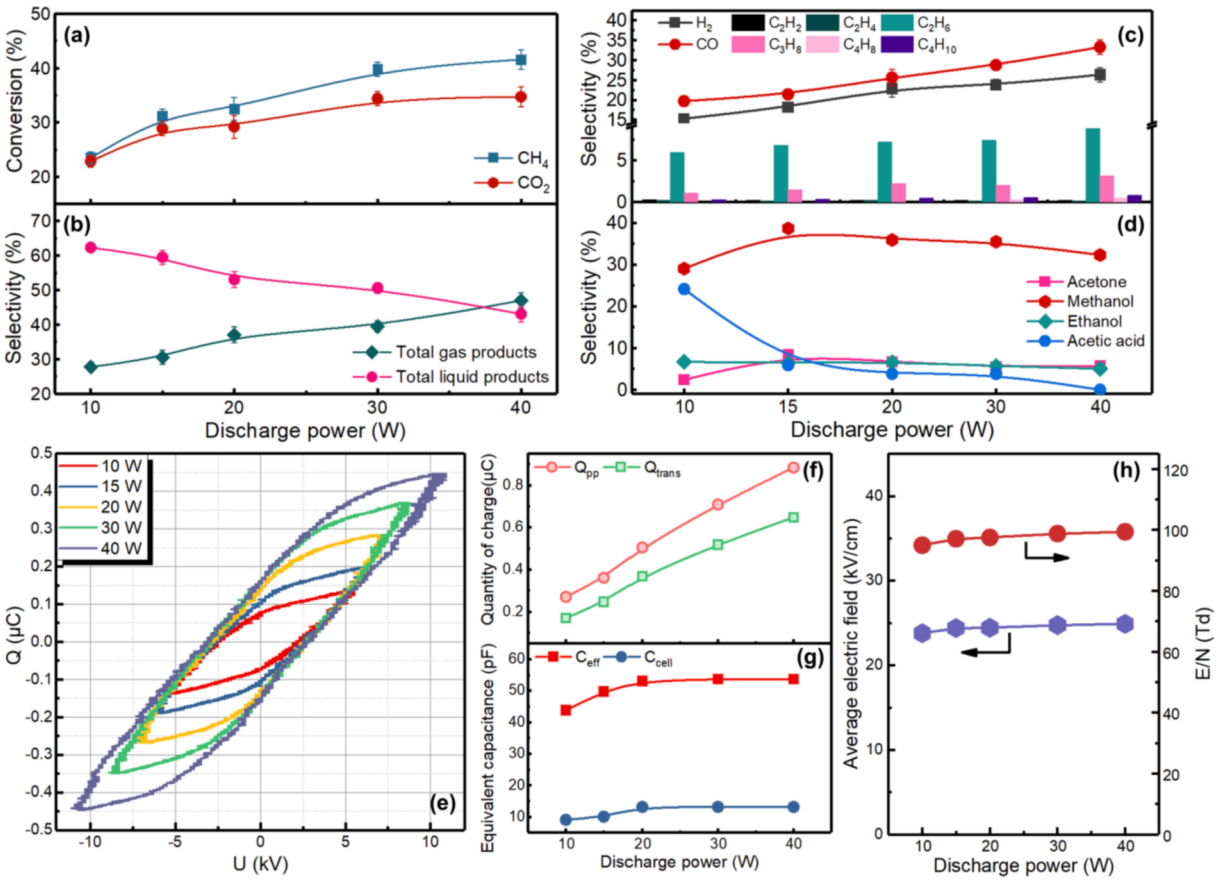

Fig. 3. Effect of different discharge powers on (a) the conversion and (b-d) the distribution of products. Influence of different discharge powers on (e) Lissajous figures, (f, g) discharge parameters, and (h) average electric fields. (flow rate: 40 mL/min; reaction temperature: 20 °C; CH_4/CO_2 = 1:1).

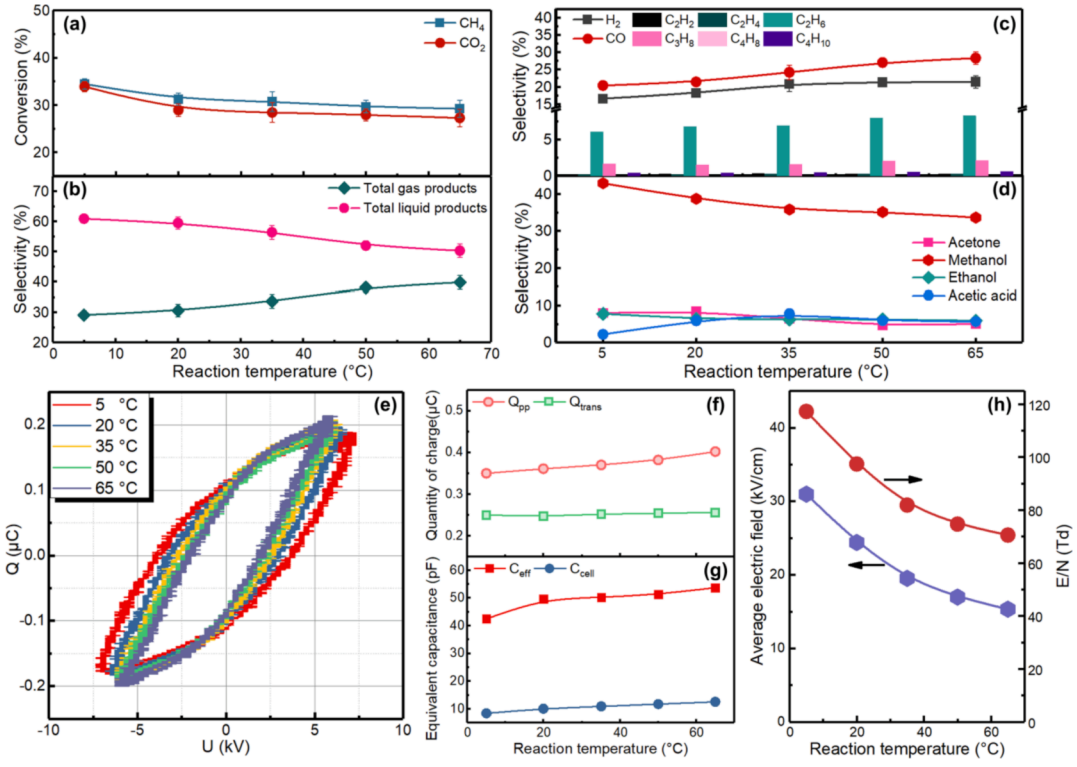

Fig. 4. Effect of different reaction temperatures on (a) the conversion and (b-d) the products distribution. Influence of different reaction temperatures on (e) Lissajous figures, (f, g) discharge parameters and (h) average electric fields. (flow rate: 40 mL/min; discharge power: 15 W; CO_2/CH_4 = 1:1).

discharge across the gap during a half-cycle of applied voltage [40], a lower C_{eff} indicates that the discharge in the gap was not fully developed at a low discharge power (e.g., less than 15 W). Increasing the discharge power to > 20 W allowed the discharge to fully develop across the discharge gap. The equivalent capacitance of the intrinsic integral DBD reactor (C_{cell}) was nearly constant at around 12 pF. Furthermore, as the breakdown voltage remained nearly constant throughout the changes in discharge power, the average electric field (E) and average reduced electric field (E/N) were maintained at ~ 24 kV/cm and 98 Td, respectively (Fig. 3h).

3.3. Effect of reaction temperature

Fig. 4a-d illustrate the influence of reaction temperature on gas conversion and product selectivity. Varying the reaction temperature from 5 to 65 °C slightly reduced the conversion of CO_2 and CH_4 by 5 – 7%, and the energy efficiency of CO_2 and CH_4 conversion decreased by 15% and 20%, respectively (Figure S4c). The product distribution was also affected by the reaction temperature, with a higher reaction temperature being unfavourable for the production of liquid products. Increasing the temperature from 5 to 65 °C decreased the total liquid product selectivity by 11%. At 5 °C, the highest methanol selectivity of 43% was achieved, with the lowest selectivities of CO (20%) and H_2 (16%). Higher reaction temperatures reduced methanol selectivity and energy efficiency by 9% and 35% (Fig. 4d and S4c), respectively, but enhanced the formation of gaseous products, especially CO and H_2. Furthermore, varying the temperature from 5 °C to 35 °C enhanced the selectivity of acetic acid from 2% to about 6%.

Interestingly, the shape of the Lissajous figure changed significantly with reaction temperature (Fig. 4e), indicating that the reaction temperature affected the discharge characteristics during the plasma reaction. Increasing the reaction temperature, as expected, reduced the peak applied voltage while increasing the density and intensity of the current pulses (Figures S5c and S5d). In addition, when the reaction temperature was raised, the peak-to-peak charge (Q_{pp}) increased by 15%, but the amount of transferred charge remained constant at 0.25 μC. Meanwhile, both C_{eff} and C_{cell} increased gradually when changing the reaction temperature from 5 °C to 65 °C, indicating that higher temperatures could improve the capacitive characteristics of the reactor and increase the charge accumulated on the dielectric surface in each cycle of the applied voltage. Increasing the reaction temperature, on the other hand, significantly reduced both E and E/N from 31 to 15 kV/cm and from 117 to 71 Td, respectively. This is due to a lower breakdown voltage at higher temperatures when maintaining a constant discharge power (20 W), as illustrated in the Lissajous figure (Fig. 4e).

3.4. Effect of residence time

Fig. 5 shows the effect of different residence times on the plasma reforming process. Increasing the residence time of the reactants from 2.1 s to 5.4 s (through the use of a lower flow rate) enhanced the conversion of CO_2 and CH_4 by 18% and 13%, respectively (Fig. 5a). The highest conversions of CO_2 and CH_4 were at around 36% each at the longest residence time of 5.4 s (28 mL/min). On the contrary, as the residence time increased, the energy efficiency of the conversion of CO_2 and CH_4 decreased, with the maximum reductions being 30% and 63% at 5.4 s, respectively (Figure S4d). The selectivity of the total liquid products increased initially with residence time and then dropped slightly as the residence time increased from 3.8 s to 5.4 s. The selectivity of the major liquid product (methanol) evolved in the same way as total liquid selectivity. When considering the balance between gas conversion and liquid selectivity, the optimal residence time for the generation of liquid products in this study was around 3.5 – 4 s. Meanwhile, changing the residence time from 2.1 to 5.4 s reduced the energy efficiency of methanol production by 25% (Figure S4d). By contrast, the CO selectivity showed the opposite trend as the total selectivity of liquids when varying the residence time. Meanwhile, the selectivity of light hydrocarbons (C_2 - C_4) reached its maximum of 11% at 2.4 s. It is worth noting that the discharge characteristics were unaffected by different residence times or gas flow rates.

4. Discussion

4.1. Electron impact reactions of CH_4 and CO_2

The electron energy distribution function (EEDF), the mean electron energy (Figure S7) and mean electron density (n_e) were calculated by the Boltzmann equation using BOLSIG+ to characterize the plasma properties at different operating parameters (discharge power or reaction temperature) [41]. As illustrated in Fig. 6a, increasing the discharge power by increasing the applied voltage at a fixed frequency had no effect on the EEDF with a constant mean electron energy of around 3.85 ± 0.05 eV, because the average electric field in the DBD reactor was almost independent of the change in discharger power.

In contrast, the mean electron density increased rapidly from 9.6×10^{16} m^{-3} to 1.6×10^{17} m^{-3} when raising the discharge power from 10 to 40 W (Fig. 6b), suggesting that a lower electron density is favorable for producing more liquid products. To provide further insights into this process, the time-averaged ICCD images are presented in Fig. 6c, showing the filamentary discharges at different discharge powers (at 20 °C). Clearly, the number of filaments generated in the discharge area

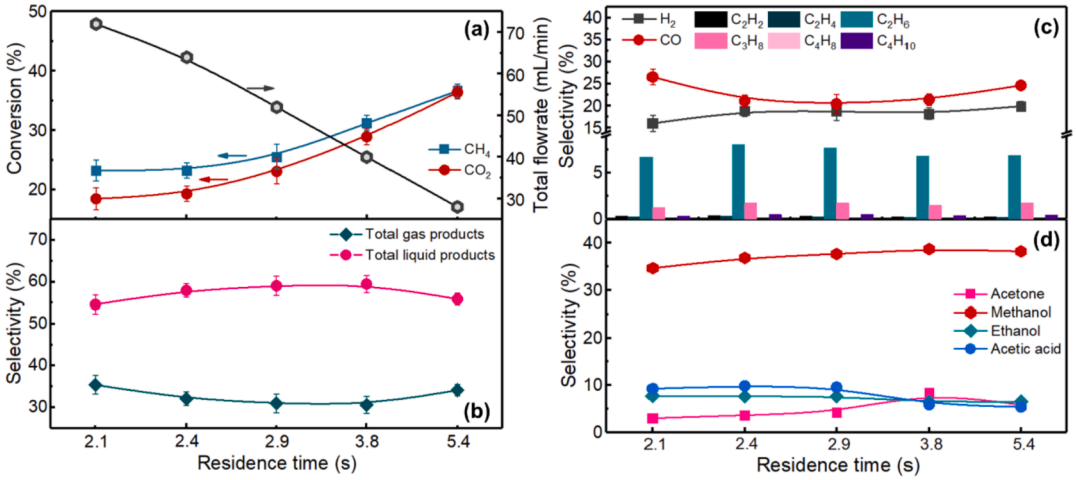

Fig. 5. Effect of different residence times on (a) the conversion and (b-d) the distribution of products (discharge power: 15 W; reaction temperature: 20 °C; CO_2/CH_4 = 1:1).

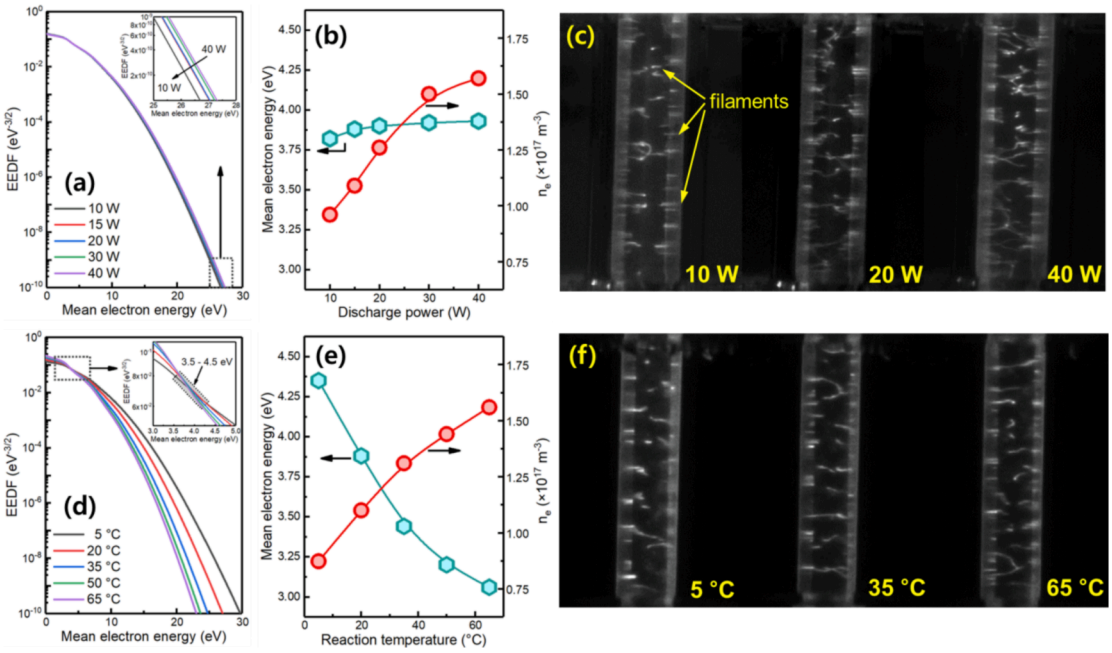

Fig. 6. Calculated electron energy distribution function (EEDF), mean electron energy and mean electron density, and ICCD images of the filamentary discharge (exposure time: 50 ms) at (a-c) different discharge powers (at a fixed temperature of 20 °C) and (d-f) different reaction temperatures (at a fixed discharge power of 15 W).

increases as discharge power increases, which could explain the increase in mean electron density. This is also consistent with the changing current pulses in the current signals (Figure S5b). This phenomenon indicates that increasing the discharge power increases the number of filamentary microdischarges, resulting in more chemical reaction channels and reactive species in the CO_2-CH_4 plasma [42], and higher conversion of CO_2 and CH_4.

As shown in Fig. 6d, higher reaction temperatures result in less generation of high energy electrons (e.g., $>$ 4.0 $\pm$ 0.5 eV). When the discharge power remained constant at 15 W, increasing the reaction temperature from 5 °C to 65 °C gradually decreased the mean electron energy from 4.4 eV to 3.1 eV, while increasing the mean electron density from 8.7 $\times$ 10^{16} m^{-3} to 1.6 $\times$ 10^{17} m^{-3} (Fig. 6e). This finding indicates that the reaction temperature influences both the mean electron energy and electron density of the DBD in the plasma DRM reaction at the same discharge powers. The corresponding variation in discharge behavior can also be observed in the ICCD images as well. At higher reaction temperatures, as shown in Fig. 6f, more filaments were generated across the gap, resulting in a higher mean electron density. Meanwhile, the discharge filaments at 5 °C were slightly brighter than those at 65 °C, implying that the intensity of each filament decreases with increasing temperature, corresponding to a decrease in mean electron energy (Fig. 6e).

Furthermore, the energy loss fraction for CO_2 and CH_4 *vs.* the reduced electric field (E/N) is displayed in Fig. 7a. As the mean electron energy did not vary with the discharge power, the distribution of energy

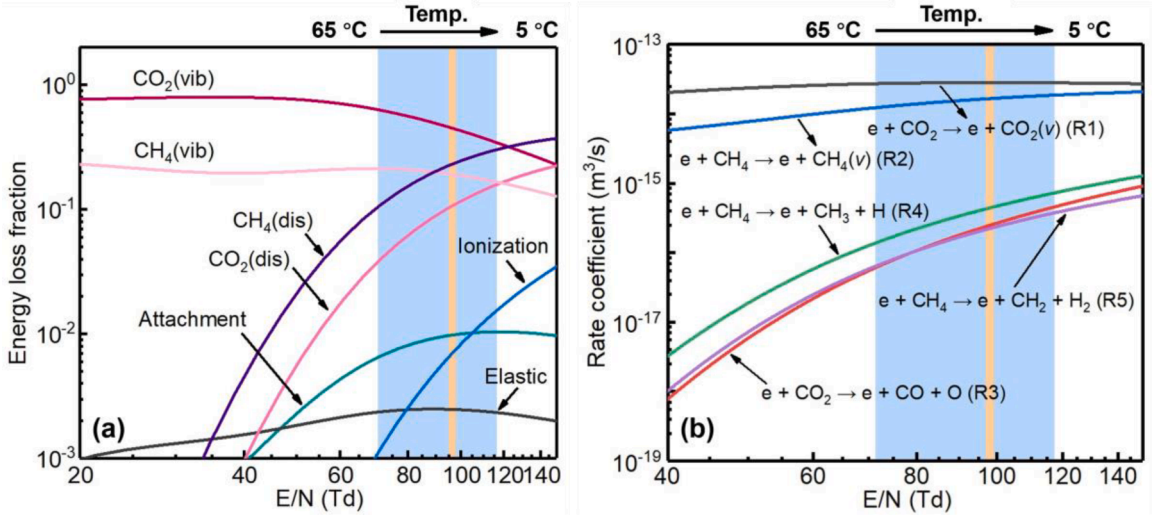

Fig. 7. (a) Electron energy loss fraction and (b) rate coefficients of electron impact reactions with CO_2 and CH_4 as a function of E/N, calculated using BOLSIG+. (CO_2 & CH_4 (vib): CO_2 & CH_4 vibrational excitation; CO_2 & CH_4 (dis): CO_2 & CH_4 dissociative excitation; Blue region: range of different reaction temperatures; Orange region: range of different discharge power.). (For interpretation of the references to colour in this figure legend, the reader is referred to the web version of this article.)

loss fractions for all reaction channels remained nearly constant when changing the discharge power (denoted by the orange region in Fig. 7a). Both vibrational and dissociative (electronic) channels are identified as the most dominant in comparison to the others (including elastic, attachment, and ionization) for the energy transfer from energetic electrons to CO_2 and CH_4, with the fraction decreasing in the order: CO_2 (vib) > CH_4 (dis) > CH_4 (vib) > CO_2 (dis). Looking at the electron energy fractions more closely, 0.45 was used for vibrational excitation of CH_4, while only 0.11 was used for dissociative excitation. The fraction of vibrational and dissociative excitations for CO_2 was 0.23 and 0.19, respectively.

When lowering the reaction temperature from 65 °C to 5 °C (denoted by the blue region in Fig. 7a), the fraction of CO_2 (dis) and CH_4 (dis) increased continuously from 0.04 to 0.16 and from 0.10 to 0.31, respectively, and surpassed the contribution of vibrational excitations (Fig. 7a). This result suggests that lower temperatures enhance both CO_2 (dis) and CH_4 (dis) channels, which is conducive to the formation of more liquid products (Fig. 4).

As the electron impact reactions are the most important CO_2 and CH_4 loss processes in a DBD plasma [43], we investigated the rate coefficients of the major electron impact reactions of CO_2 and CH_4 as a function of the reduced electric field (E/N), as shown in Fig. 7b. In general, the rate coefficients of all reactions increase as E/N in the plasma increases. In this work, the reaction rate coefficients for the vibrational excitation of CO_2 and CH_4 (R1 & R2), as the dominant electron impact reactions, were almost constant at different operating parameters including discharge power and reaction temperature, suggesting that these vibration excitation processes have little influence on the product distribution. For CO_2, the electron impact vibrational excitation (R1) of the lowest vibrational level may result in further vibrational-vibrational (V-V) collisions, gradually progressing to a higher vibrational level (known as a "ladder-climbing" process) until the dissociation of the CO_2 molecules; this reaction pathway is also known to have a higher energy efficiency for CO_2 conversion under plasma conditions, since this dissociation process only requires a minimum energy of 5.5 eV [44,45]. Meanwhile, the rate coefficient of electron impact dissociation of CH_4 to CH_3 (R4) was higher than that of CH_2 formation (R5) and CO_2 dissociation (R3). Lowering the reaction temperature from 65 °C to 5 °C increased the rate coefficients of these three reactions could increase by a factor of 1.3 – 5.3, demonstrating that lower temperatures could promote the formation of radicals and atoms, such as CO, O, H, and CH_x, etc.

As reported using 0D plasma modeling [46–48], methanol (CH_3OH), confirmed as the major liquid product in our experiments, can be derived mainly through the three-body reaction (R6) between CH_3 and OH [1,47]. At lower temperatures, the formation of CH_3 is enhanced through R4 by a higher E/N (see Fig. 7b), which can explain the higher CH_3OH formation at lower temperatures observed in our experiments.

$$CH_3 + OH + M \rightarrow CH_3OH + M,\ M = CH_4 \text{ or } CO_2 \quad (R6)$$

In addition, CH_3OH in plasma can be produced by the partial oxidation of methane via radical reactions between $O(^1D)$ and CH_4 (R7 – R9) [49,50], where $O(^1D)$ is primarily produced via electron impact dissociation of CO_2 (R10) [1] and electron impact excitation of O (R11) [48], respectively. These O atoms are in turn mainly produced by electron impact dissociation of CO_2 ((R3) in Fig. 7b). Reaction (R10) follows a similar E/N dependence as (R3) (see Fig. 7b), which can explain the higher CH_3OH formation observed in our experiments at lower temperatures.

$$O(^1D) + CH_4 \rightarrow CH_3OH \quad (R7)$$

$$O(^1D) + CH_4 \rightarrow CH_3O \text{ or } CH_2OH + H \rightarrow CH_3OH \quad (R8)$$

$$O(^1D) + CH_4 \rightarrow CH_2O + H_2 \rightarrow CH_3OH \quad (R9)$$

$$e^- + CO_2 \rightarrow e^- + CO + O(^1D) \quad (R10)$$

$$e^- + O \rightarrow e^- + O(^1D) \quad (R11)$$

Furthermore, acetic acid is obtained as one of the major oxygenates at a low discharge power of 10 W, and it can be directly formed by the recombination of CH_3 and carboxyl radicals (R12) as confirmed by DFT calculations [51]. Furthermore, COOH radicals can also be formed by the coupling of CO and OH (R13) with a low energy barrier (0.2 eV) [51,52].

$$CH_3 + COOH \rightarrow CH_3COOH \quad (R12)$$

$$CO + OH \rightarrow COOH \quad (R13)$$

Therefore, the formation of oxygenates, such as methanol and acetic acid, is strongly related to gaseous reactions involving key radicals, such as CH_3, OH, $O(^1D)$, H, and also CO, whose formation is strongly aided by higher electron energies at lower temperatures.

4.2. Optical emission spectroscopic diagnostics

Emission spectra of the CO_2-CH_4 plasma were recorded to better understand the formation of gas-phase reactive species (Fig. 8a and Table S1). The emission spectra of the deexcitation channels prove the presence of a variety of reactive excited species and their corresponding low-energy (including ground) states, such as CO_2, CO_2^+, CO, CO^+, CH, C_2, OH, and H.

The CO ($B^1\Sigma - A^1\Pi$) and CO ($b^3\Sigma_{2u} - a^3\Pi_{1g}$) bands prove the presence of several singlet and triplet CO electronic excited states in the plasma, such as $B^1\Sigma$ (10.8 eV), $A^1\Pi$ (8.0 eV), $b^3\Sigma$ (10.4 eV), and $a^3\Pi$ (6.0 eV) (Fig. 8b). Furthermore, the CO $a^3\Pi$ state could contribute to the formation of C_2 (R14), as evidenced by the presence of the C_2 Swan band ($d^2\Pi - a^3\Pi$) in the spectra.

$$CO\ (a^3\Pi) + C \rightarrow C_2 + O \quad (R14)$$

Meanwhile, the deexcitation processes of the electronically excited species CH ($A^2\Delta$, $B^2\Sigma$, $C^2\Sigma^+$) to the ground state ($X^2\Pi$) are visible in the spectrum, illustrating that there could be multiple parallel transformation channels for the formation of CH species with the states of $A^2\Delta$ (12.1 eV), $B^2\Sigma$ (12.5 eV), $C^2\Sigma^+$ (13.3 eV), respectively (Fig. 8b). Furthermore, the appearance of these CH states and excited H (3d) indicates that CH_4 molecules in the plasma could be excited to extremely high excited states (Super excited states, 16.6 eV). We propose a stepwise multichannel dissociation of CH_4 based on the excitations of the fragments CH and H, namely $CH_4 \rightarrow CH_3 + H$ (R4) $\rightarrow CH_2 + 2H \rightarrow CH + 3H$, and $CH_4 \rightarrow CH_2 + 2H$ (R5) $\rightarrow CH + 3H$ (Fig. 7b).

As shown in Fig. 8c and S8, different discharge powers and reaction temperatures could influence the fluorescence intensity of particular excited radicals, including, CH, CO, OH, and H undergoing different deexcitations. All of the peak intensities caused by deexcitations of these four excited radicals rose monotonically with the increasing discharge power, which could be due to a higher electron density producing more excited species. When compared to CO ($B^1\Sigma - A^1\Pi$), the intensity of the CO ($b^3\Sigma - a^3\Pi$) band grew at a much faster rate, indicating that the collision-induced intersystem crossing process (R15) could be accelerated at a higher electron density. At different reaction temperatures, a lower mean electron energy (E_e) could simultaneously reduce the growth rate of CO ($b^3\Sigma - a^3\Pi$) and the Angstrom emission.

$$CO\ (B^1\Sigma) + M \rightarrow CO\ (b^3\Sigma) + M \quad (R15)$$

On the other hand, increasing the reaction temperature from 5 °C to 65 °C decreased the intensities of CH ($C^2\Sigma^+ - X^2\Pi$), CH ($B^2\Sigma - X^2\Pi$), CH ($A^2\Delta - X^2\Pi$), OH ($B^1\Sigma - A^1\Pi$), and H (3d – 2p), which could be attributed to a decrease in mean electron energy. Notably, when compared to the effect of different powers, changing the reaction temperature resulted in a similar range and trend of electron density but a decrease in mean electron energy. Thus, the density of the excited radicals can be determined by mean electron energy and mean electron density

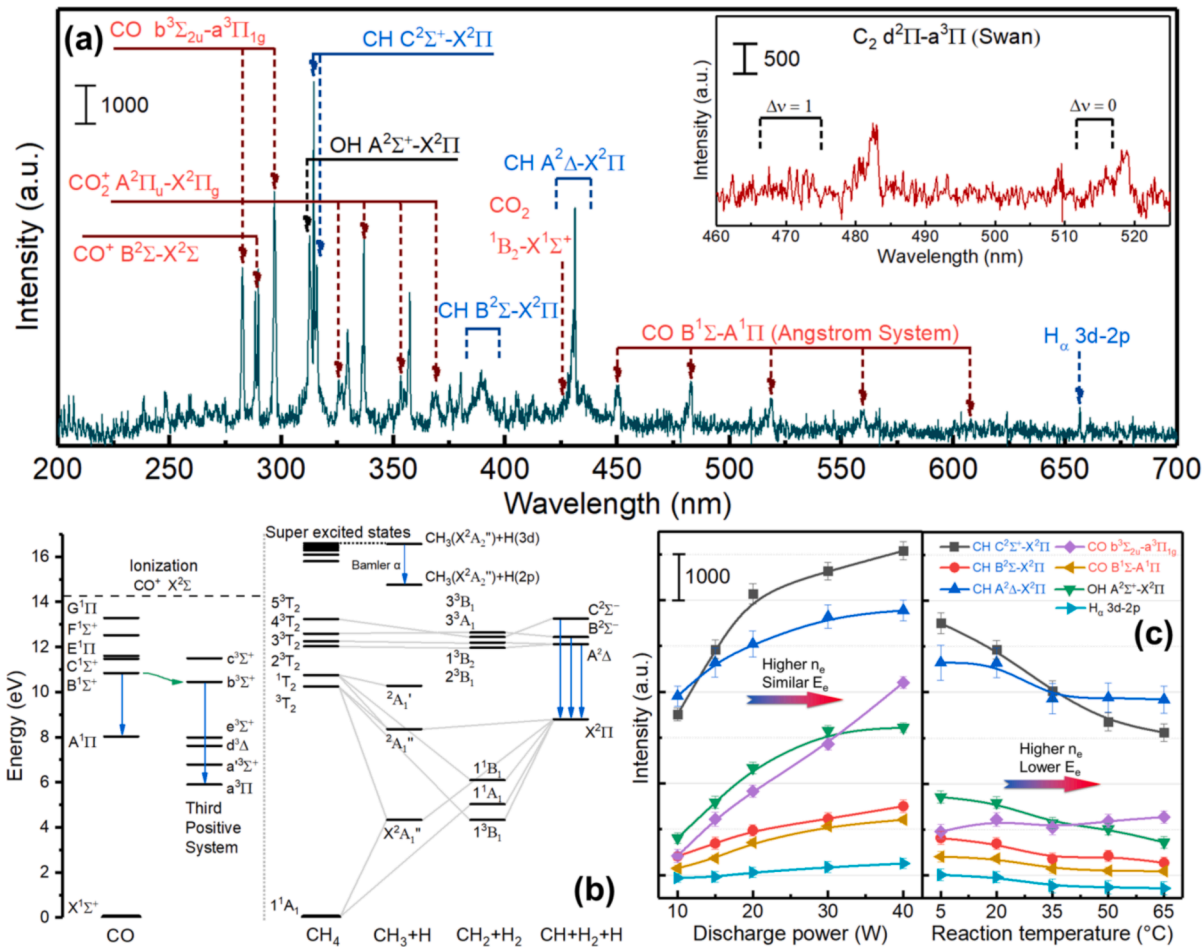

Fig. 8. (a) Typical optical emission spectra for the CO_2-CH_4 plasma (discharge power: 40 W). (b) Electronic energy levels and terms for CO and CH_4 (including dissociation), as reproduced from literatures[53–55]. The blue arrows indicate the detected emissions; the green arrow denotes the collision-induced intersystem crossing. (c) Effect of discharge power and reaction temperature on the intensity of different emission lines, originating from various excited species in the CO_2-CH_4 plasma derived from Figure S4 (CH($C^2\Sigma^+ - X^2\Pi$) 314 nm; CH($B^2\Sigma - X^2\Pi$) 387 nm; CH($A^2\Delta - X^2\Pi$) 431 nm; OH($A^2\Sigma^+ - X^2\Pi$) 309 nm; CO($b^3\Sigma_{2u} - a^3\Pi_{1g}$) 283 nm; CO ($B^1\Sigma - A^1\Pi$) 451 nm; H_α(3d – 2p) 656 nm). (For interpretation of the references to colour in this figure legend, the reader is referred to the web version of this article.)

simultaneously. Furthermore, when the discharge power and reaction temperature were changed, CH ($A^2\Delta$, $B^2\Sigma$, $C^2\Sigma^+ - X^2\Pi$), and CO ($B^1\Sigma - A^1\Pi$) exhibited the same variation trend as the CH_4 and CO_2 conversions. However, there was no obvious relationship between the emission intensity of excited radicals and the selectivity of products, indicating that the plasma properties could affect the excitation of gas-phase radicals, but were not the decisive factor for the product distribution, which would be influenced by the interaction of multiple factors.

4.3. Importance and coupling effect of process parameters

Due to the high complexity of the plasma DRM process, two typical ANN models (ANN_1 and ANN_2) were developed to predict the reaction performance (including "conversion & selectivity" and "energy efficiency") of the plasma-enhanced DRM process at different process parameters and key discharge indicators of plasma reaction, respectively (Figures S2a and S3a).

The predicted results from both models were consistent with the corresponding experimental data as the correlation coefficient (R^2) of both ANN models was ~ 0.999 (Figures S2b and S2c, Figure S3b, and Figure S9).

Fig. 9a shows the relative importance of different process parameters to the conversion & selectivity. The discharge power was found to be the most critical parameter affecting both the conversion and product selectivity. In addition, discharge power had a more significant effect on CO_2 conversion than on CH_4 conversion. In comparison to other gas and liquid products, the production of H_2 and methanol (selectivity) was more dependent on discharge power. In addition, we found that the reaction temperature had the least influence on the formation of gaseous products. Notably, when compared to the major gaseous products, the liquid products were less affected by the reaction temperature or residence time with a combined importance of less than 50%. On the other hand, the discharge power was also identified as the most critical process parameter in determining the energy efficiency of the plasma DRM process with a relative importance of 53% – 72%. The reaction temperature is the least important process parameter to the energy efficiency for the production of gaseous products, while the residence time is the least important in terms of the energy efficiency for the production of liquid products except for acetone.

Fig. 9b exhibits the possible relationships among the process parameters, discharge parameters, and process performance. The mean electron energy (E_e), mean electron density (n_e), and specific energy input (SEI) are selected as the key discharge indicators to characterize the discharge properties of the plasma DRM process. As shown in Fig. 6b, raising the discharge power increases both n_e and SEI simultaneously, with the SEI also being influenced by the residence time (or total gas flow rate). Furthermore, varying the reaction temperature could tailor the key discharge indicators (E_e, n_e, & SEI) synchronously, all of which could have a synergistic effect on the product distribution. Fig. 9c shows that the SEI is the most important discharge parameter (47 – 51%)

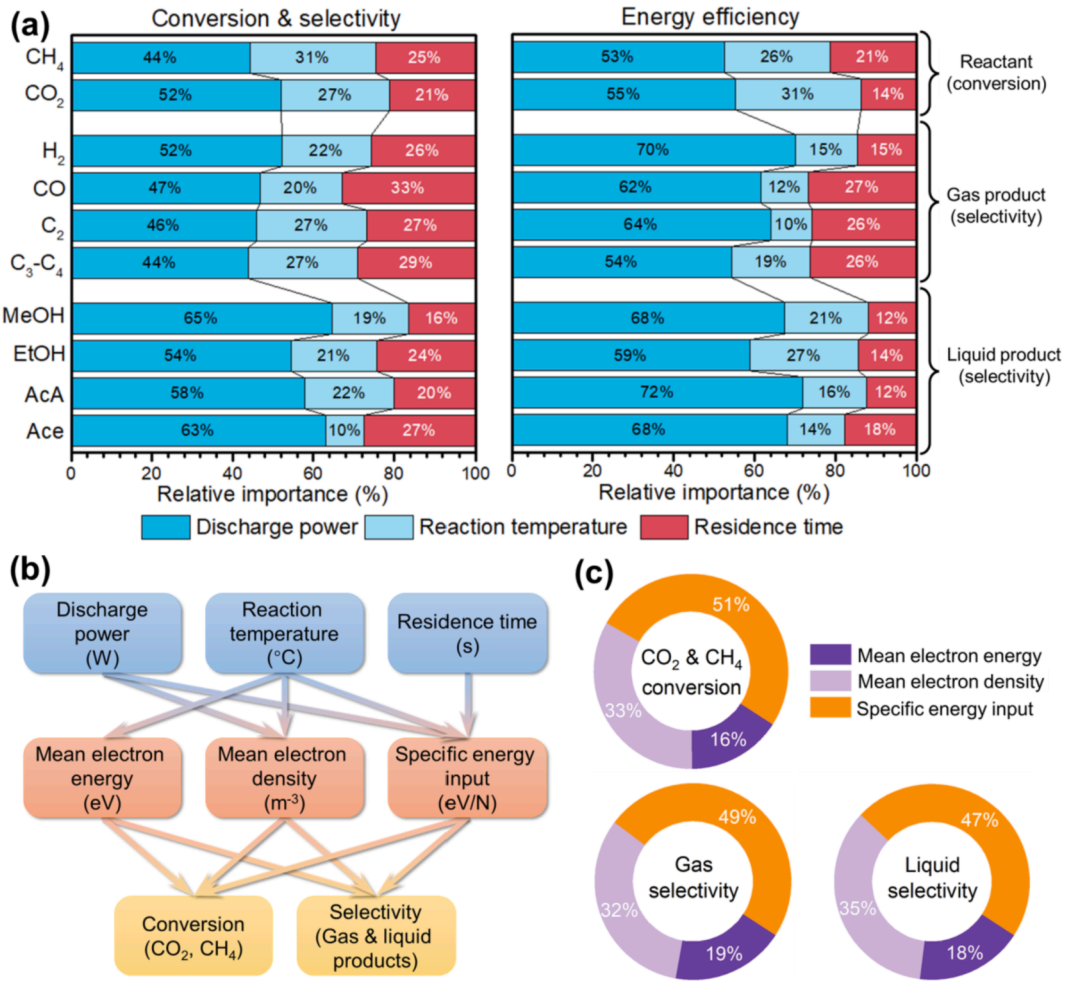

Fig. 9. (a) Importance analysis of conversion & selectivity and energy efficiency based on discharge power, reaction temperature and residence time. (MeOH: methanol; EtOH: ethanol; AcA: acetic acid; Ace: acetone) (b) Scheme of the possible relationship of process parameters (blue), key indicators of plasma-driven DRM reaction (red), and performance (yellow). (The arrows represent the underlying relationships between two key elements that are linked) (c) Importance analysis of reaction performance based on key discharge indicators. (For interpretation of the references to colour in this figure legend, the reader is referred to the web version of this article.)

affecting the conversion and selectivity of gaseous and liquid products, respectively, followed by the mean electron density (32 – 35%) and mean electron energy (16 – 19%), which suggests that all these key indicators could have a certain impact on the reaction performance. Interestingly, the relative contribution of these three key indicators is quite similar for both the gas conversion and product selectivity (Fig. 9c and Figure S10). These findings also indicate that discharge power and residence time (or flow rate) are relatively more independent parameters than reaction temperature, making them more controllable so that they can be tuned to achieve the desirable performance in a practical process.

Furthermore, the 3D plots of the predicted results from the optimized ANN_1 model show the simultaneous effects of discharge power, reaction temperature, and residence time on the reaction performance (Figure S11). At a discharge power of 40 – 50 W and a reaction temperature in the range of 5 – 35 °C, the conversion of CH_4 and CO_2 can reach over 45% and 40%, respectively at a residence time of > 5 s. Meanwhile, the results of ANN_1 show that increasing the discharge power and reaction temperature simultaneously promotes the selectivity of major gaseous products (CO and H_2). Methanol, as the major liquid product, have a selectivity of over 40% at 20 W and 5 °C with a suitable range of residence times (2 – 5 s). Meanwhile, we find that a lower discharge power (10 W) is beneficial for achieving a higher selectivity of acetic acid (~ 35%), whereas a combination of low discharge power with a 2 s residence time at a lower temperature can promote the formation of ethanol. Furthermore, higher hydrocarbons ($C_2 – C_4$) are more likely to form at higher discharge power and reaction temperature. Therefore, the generation of oxygenates, particularly for methanol, can be enhanced under optimal operating conditions such as low discharge power (10 – 20 W) with shorter residence time and lower reaction temperature.

As shown in Figure S12, the energy efficiency for the conversion of CO_2 and CH_4 is mainly influenced by the discharge power, while a lower discharge power (10 – 20 W) is favorable for achieving higher energy efficiency. Notably, both lower discharge power and shorter residence time can both lead to higher energy efficiency in the production of primary products. At a discharge power of 10 W and a residence time of 2 s, the energy efficiency reaches its peak for the production of CO (1.1 mol/kWh) and methanol (1.3 mol/kWh) at 65 °C and 5 °C, respectively. Furthermore, the energy efficiency for H_2 production (0.4 mol/kWh) can be maintained at a residence time of 2 – 3 s.

In this work, two non-dimensional indexes, I_1 and I_2, were introduced to optimize process parameters to balance reaction performance (conversion & selectivity) and energy efficiency, as displayed in Fig. 10. To obtain a higher I_1, the optimized discharge power and reaction temperature ranges are 10 – 20 W and 5 – 20 °C, respectively. For primary products, a shorted residence time with a higher I_2 can enhance both selectivity and energy efficiency simultaneously. H_2 production can

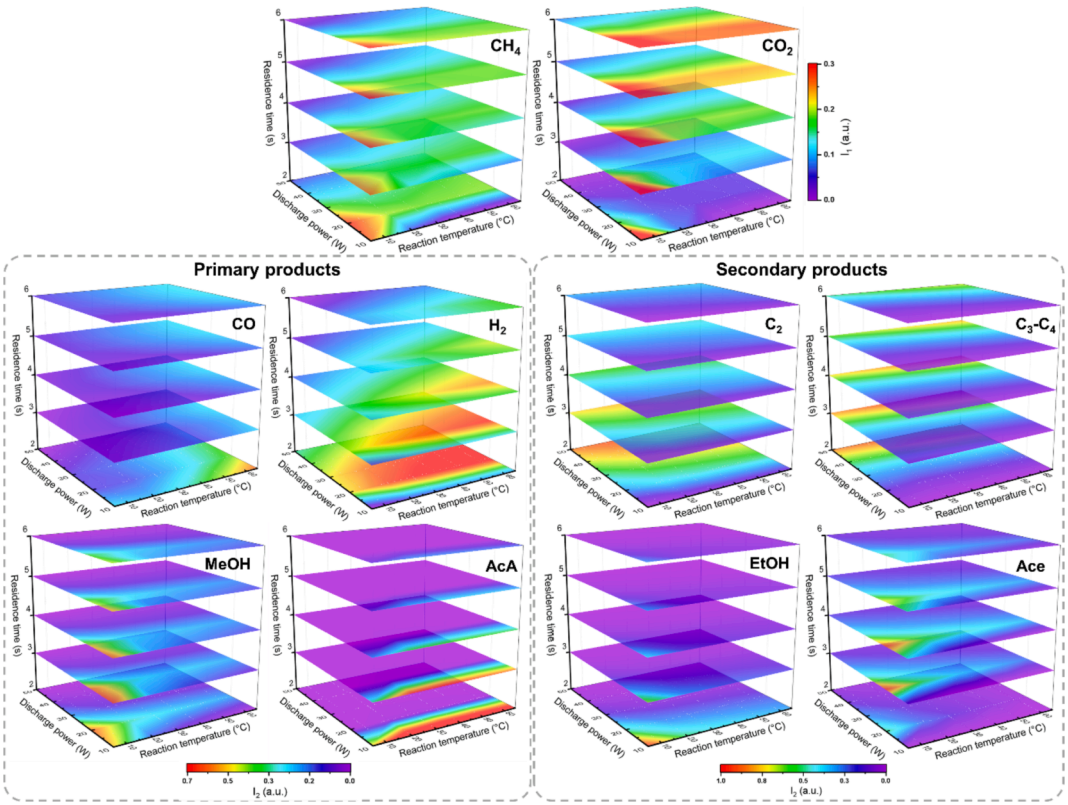

Fig. 10. Prediction results of the coupled effects of the three parameters, including discharge power, reaction temperature and residence time, on the comprehensive evaluation indices of (a) I_1 for CH_4 and CO_2 conversion, and I_2 for (b) primary (H_2, CO, methanol (MeOH) and acetic acid (AcA)) and (c) secondary products (C_2, C_3 - C_4, ethanol (EtOH) and acetone (Ace)).

be promoted at a relatively high I_2 (> 0.6) when the discharge power and temperature are in the optimal ranges of 20 – 30 W and 35 – 65 °C, respectively. At a residence time of 2 s, a power of 10 W and a temperature of 65 °C are the best operating conditions for CO production, while methanol production is more favorable at a low temperature (5 °C) with a discharge power of 20 W. Another major oxygenate, acetic acid, is preferably produced at a low discharge power of 10 W, especially at optimal temperatures (20 – 50 °C) and residence time (2 – 3 s).

5. Conclusion

Herein, we report a catalyst-free single-step approach for the synthesis of oxygenates through the plasma-driven DRM reaction in a temperature-controlled DBD reactor. The product distribution can be tuned by changing the process parameters including the CO_2/CH_4 ratio, discharge power, reaction temperature, and residence time. The highest methanol selectivity of 43% was attained at 5 °C and 15 W, while a lower discharge power (10 W) was favorable for the production of acetic acid at room temperature (20 °C). The selectivity of gaseous products, mainly H_2 and CO, increased when the discharge power and reaction temperature were increased. We revealed the correlation between different process parameters (discharge power, reaction temperature, and residence time) and the key discharge properties simultaneously, including mean electron energy (E_e), electron density (n_e), and specific energy input (SEI). A higher discharge power can result in a higher mean electron density but a similar mean electron energy, whereas varying the reaction temperature can affect both the mean electron energy and electron density. In addition, a low reaction temperature combined with a high electron energy can significantly promote the electron impact reactions of CO_2 and CH_4. Moreover, two well-trained ANN models were developed to comprehend the relative importance of process parameters (ANN_1) and key discharge indicators (ANN_2) on reaction performance. Compared to reaction temperature and residence time, discharge power is identified as the most critical process parameter influencing reforming performance. The results of the ANN models show that higher conversions of CO_2 and CH_4 with better energy efficiencies can be achieved at 10 – 20 W and 5 – 20 °C. Furthermore, methanol production could be optimized with a selectivity of over 40% alongside an energy efficiency of over 0.8 mol/kWh under suitable conditions (20 W, 5 °C, and 2 s). This work demonstrates that the direct transformation of CH_4 and CO_2 into oxygenates can be tuned and optimized for the selective synthesis of target liquid products (e.g., methanol), showing great potential to address the challenges of global warming and climate change.

Declaration of Competing Interest

The authors declare that they have no known competing financial interests or personal relationships that could have appeared to influence the work reported in this paper.

Data availability

Data will be made available on request.

Acknowledgements

This project received funding from the European Union's Horizon 2020 research and innovation program under the Marie Sklodowska-Curie grant agreement No. 813393.

Appendix A. Supplementary data

Supplementary data to this article can be found online at https://doi.org/10.1016/j.cej.2022.137860.

References

[1] S. Liu, L.R. Winter, J.G. Chen, Review of plasma-assisted catalysis for selective generation of oxygenates from CO_2 and CH_4, ACS Catal. 10 (2020) 2855–2871, https://doi.org/10.1021/acscatal.9b04811.

[2] R. Snoeckx, A. Bogaerts, Plasma technology-a novel solution for CO_2 conversion? Chem. Soc. Rev. 46 (2017) 5805–5863, https://doi.org/10.1039/c6cs00066e.

[3] A. George, B. Shen, M. Craven, Y. Wang, D. Kang, C. Wu, X. Tu, A review of non-thermal plasma technology: A novel solution for CO_2 conversion and utilization, Renew. Sustain. Energy Rev. 135 (2021), 109702, https://doi.org/10.1016/j.rser.2020.109702.

[4] G. Chen, R. Snyders, N. Britun, CO_2 conversion using catalyst-free and catalyst-assisted plasma-processes: Recent progress and understanding, J. CO2 Util. 49 (2021), 101557, https://doi.org/10.1016/j.jcou.2021.101557.

[5] Y. Sun, J. Wu, Y. Wang, J. Li, N. Wang, J. Harding, S. Mo, L. Chen, P. Chen, M. Fu, D. Ye, J. Huang, X. Tu, Plasma-catalytic CO_2 hydrogenation over a Pd/ZnO catalyst. In Situ probing of gas-phase and surface reactions, JACS Au (2022), https://doi.org/10.1021/jacsau.2c00028.

[6] G. Chen, X. Tu, G. Homm, A. Weidenkaff, Plasma pyrolysis for a sustainable hydrogen economy, Nat. Rev. Mater. 7 (2022) 333–334, https://doi.org/10.1038/s41578-022-00439-8.

[7] Y. Wang, W. Yang, S. Xu, S. Zhao, G. Chen, A. Weidenka, C. Hardacre, X. Fan, J. Huang, X. Tu, Shielding protection by mesoporous catalysts for improving plasma-catalytic ambient ammonia synthesis, J. Am. Chem. Soc. (2022), https://doi.org/10.1021/jacs.2c01950.

[8] D. Li, X. Li, M. Bai, X. Tao, S. Shang, X. Dai, Y. Yin, CO_2 reforming of CH_4 by atmospheric pressure glow discharge plasma: a high conversion ability, Int. J. Hydrogen Energy. 34 (2009) 308–313, https://doi.org/10.1016/j.ijhydene.2008.10.053.

[9] B. Wanten, S. Maerivoet, C. Vantomme, J. Slaets, G. Trenchev, A. Bogaerts, Dry reforming of methane in an atmospheric pressure glow discharge: Confining the plasma to expand the performance, J. CO2 Util. 56 (2022), 101869, https://doi.org/10.1016/j.jcou.2021.101869.

[10] A. Aziznia, H.R. Bozorgzadeh, N. Seyed-Matin, M. Baghalha, A. Mohamadalizadeh, Comparison of dry reforming of methane in low temperature hybrid plasma-catalytic corona with thermal catalytic reactor over Ni/γ-Al_2O_3, J. Nat. Gas Chem. 21 (2012) 466–475, https://doi.org/10.1016/S1003-9953(11)60392-7.

[11] S.M. Chun, Y.C. Hong, D.H. Choi, Reforming of methane to syngas in a microwave plasma torch at atmospheric pressure, J. CO2 Util. 19 (2017) 221–229, https://doi.org/10.1016/j.jcou.2017.03.016.

[12] K. Li, J.L. Liu, X.S. Li, H.Y. Lian, X. Zhu, A. Bogaerts, A.M. Zhu, Novel power-to-syngas concept for plasma catalytic reforming coupled with water electrolysis, Chem. Eng. J. 353 (2018) 297–304, https://doi.org/10.1016/j.cej.2018.07.111.

[13] S. Van Alphen, F. Jardali, J. Creel, G. Trenchev, R. Snyders, A. Bogaerts, Sustainable gas conversion by gliding arc plasmas: a new modelling approach for reactor design improvement, Sustain, Energy Fuels. 5 (2021) 1786–1800, https://doi.org/10.1039/d0se01782e.

[14] J.A. Andersen, J.M. Christensen, M. Østberg, A. Bogaerts, A.D. Jensen, Plasma-catalytic dry reforming of methane: Screening of catalytic materials in a coaxial packed-bed DBD reactor, Chem. Eng. J. 397 (2020), 125519, https://doi.org/10.1016/j.cej.2020.125519.

[15] Z. Ye, J. Yang, N. Zhong, X. Tu, J. Jia, J. Wang, Tackling environmental challenges in pollution controls using artificial intelligence: A review, Sci. Total Environ. 699 (2020), 134279, https://doi.org/10.1016/j.scitotenv.2019.134279.

[16] Z. Sheng, Y. Watanabe, H.H. Kim, S. Yao, T. Nozaki, Plasma-enabled mode-selective activation of CH_4 for dry reforming: First touch on the kinetic analysis, Chem. Eng. J. 399 (2020), 125751, https://doi.org/10.1016/j.cej.2020.125751.

[17] Y. Uytdenhouwen, K.M. Bal, E.C. Neyts, V. Meynen, P. Cool, A. Bogaerts, On the kinetics and equilibria of plasma-based dry reforming of methane, Chem. Eng. J. 405 (2021), 126630, https://doi.org/10.1016/j.cej.2020.126630.

[18] X. Wang, Y. Gao, S. Zhang, H. Sun, J. Li, T. Shao, Nanosecond pulsed plasma assisted dry reforming of CH_4: The effect of plasma operating parameters, Appl. Energy. 243 (2019) 132–144, https://doi.org/10.1016/j.apenergy.2019.03.193.

[19] Y. Uytdenhouwen, J. Hereijgers, T. Breugelmans, P. Cool, A. Bogaerts, How gas flow design can influence the performance of a DBD plasma reactor for dry reforming of methane, Chem. Eng. J. 405 (2021), 126618, https://doi.org/10.1016/j.cej.2020.126618.

[20] A.H. Khoja, M. Tahir, N.A.S. Amin, Dry reforming of methane using different dielectric materials and DBD plasma reactor configurations, Energy Convers. Manag. 144 (2017) 262–274, https://doi.org/10.1016/j.enconman.2017.04.057.

[21] Y. Xia, N. Lu, B. Wang, J. Li, K. Shang, N. Jiang, Y. Wu, Dry reforming of CO_2–CH_4 assisted by high-frequency AC gliding arc discharge: Electrical characteristics and the effects of different parameters, Int. J. Hydrogen Energy. 42 (2017) 22776–22785, https://doi.org/10.1016/j.ijhydene.2017.07.104.

[22] Y. Wang, L. Yao, S. Wang, D. Mao, C. Hu, Low-temperature catalytic CO_2 dry reforming of methane on Ni-based catalysts: A review, Fuel Process. Technol. 169 (2018) 199–206, https://doi.org/10.1016/j.fuproc.2017.10.007.

[23] G. Scarduelli, G. Guella, D. Ascenzi, P. Tosi, Synthesis of liquid organic compounds from CH_4 and CO_2 in a dielectric barrier discharge operating at atmospheric pressure, Plasma Process. Polym. 8 (2011) 25–31, https://doi.org/10.1002/ppap.201000044.

[24] N. Bouchoul, E. Fourré, J.M. Tatibouët, C. Batiot-Dupeyrat, Plasma-catalytic dry reforming of CH_4 over calcium oxide: Catalyst structural and textural modifications, Plasma Chem. Plasma Process. 39 (2019) 713–727, https://doi.org/10.1007/s11090-019-09966-9.

[25] V. Goujard, J.M. Tatibouët, C. Batiot-Dupeyrat, Carbon dioxide reforming of methane using a dielectric barrier discharge reactor: Effect of helium dilution and kinetic model, Plasma Chem. Plasma Process. 31 (2011) 315–325, https://doi.org/10.1007/s11090-010-9283-y.

[26] V. Goujard, J.M. Tatibouët, C. Batiot-Dupeyrat, Use of a non-thermal plasma for the production of synthesis gas from biogas, Appl. Catal. A Gen. 353 (2009) 228–235, https://doi.org/10.1016/j.apcata.2008.10.050.

[27] J.J. Zou, Y.P. Zhang, C.J. Liu, Y. Li, B. Eliasson, Starch-enhanced synthesis of oxygenates from methane and carbon dioxide using dielectric-barrier discharges, Plasma Chem. Plasma Process. 23 (2003) 69–82, https://doi.org/10.1023/A:1022416819132.

[28] Y.P. Zhang, Y. Li, Y. Wang, C.J. Liu, B. Eliasson, Plasma methane conversion in the presence of carbon dioxide using dielectric-barrier discharges, Fuel Process. Technol. 83 (2003) 101–109, https://doi.org/10.1016/S0378-3820(03)00061-4.

[29] L. Wang, Y. Yi, C. Wu, H. Guo, X. Tu, One-step reforming of CO_2 and CH_4 into high-value liquid chemicals and fuels at room temperature by plasma-driven catalysis, Angew. Chemie - Int. Ed. 56 (2017) 13679–13683, https://doi.org/10.1002/anie.201707131.

[30] Y. Li, C.-J.-J. Liu, B. Eliasson, Y. Wang, Synthesis of oxygenates and higher hydrocarbons directly from methane and carbon dioxide using dielectric-barrier discharges: product distribution, Energy Fuels 16 (2002) 864–870, https://doi.org/10.1021/ef0102770.

[31] Y. Wang, L. Fan, H. Xu, X. Du, H. Xiao, J. Qian, Y. Zhu, X. Tu, L. Wang, Insight into the synthesis of alcohols and acids in plasma-driven conversion of CO_2 and CH_4 over copper-based catalysts, Appl. Catal. B Environ. 315 (2022), 121583, https://doi.org/10.1016/j.apcatb.2022.121583.

[32] L. Wang, Y. Yi, H. Guo, X. Tu, Atmospheric pressure and room temperature synthesis of methanol through plasma-catalytic hydrogenation of CO_2, ACS Catal. 8 (2018) 90–100, https://doi.org/10.1021/acscatal.7b02733.

[33] Y. Wang, M. Craven, X. Yu, J. Ding, P. Bryant, J. Huang, X. Tu, Plasma-enhanced catalytic synthesis of ammonia over a Ni/Al_2O_3 catalyst at near-room temperature: Insights into the importance of the catalyst surface on the reaction mechanism, ACS Catal. 9 (2019) 10780–10793, https://doi.org/10.1021/acscatal.9b02538.

[34] Y. Wang, Z. Liao, S. Mathieu, F. Bin, X. Tu, Prediction and evaluation of plasma arc reforming of naphthalene using a hybrid machine learning model, J. Hazard. Mater. 404 (2021) 123965, https://doi.org/10.1016/j.jhazmat.2020.123965.

[35] S.Y. Liu, D.H. Mei, Z. Shen, X. Tu, Nonoxidative conversion of methane in a dielectric barrier discharge reactor: Prediction of reaction performance based on neural network model, J. Phys. Chem. C. 118 (2014) 10686–10693, https://doi.org/10.1021/jp502557s.

[36] J. Heaton, S. Mcelwee, J. Fraley, J. Cannady, Early stabilizing feature importance for tensorFlow deep neural networks, 2017 International Joint Conference on Neural Networks (IJCNN) (2017) 4618–4624, https://doi.org/10.1109/IJCNN.2017.7966442.

[37] S.K. Das, P.K. Basudhar, Prediction of residual friction angle of clays using artificial neural network, Eng. Geol. 100 (2008) 142–145, https://doi.org/10.1016/j.enggeo.2008.03.001.

[38] Z. Zhang, M.W. Beck, D.A. Winkler, B. Huang, W. Sibanda, Opening the black box of neural networks : methods for interpreting neural network models in clinical applications, Ann. Tansl. Med. 6 (2018) 216, https://doi.org/10.21037/atm.2018.05.32.

[39] D. Mei, Y.Y. He, S. Liu, J. Yan, X. Tu, Optimization of CO_2 conversion in a cylindrical dielectric barrier discharge reactor using design of experiments, Plasma Process. Polym. 13 (2016) 544–556, https://doi.org/10.1002/ppap.201500159.

[40] X. Tu, H.J. Gallon, M. V. Twigg, P.A. Gorry, J.C. Whitehead, Dry reforming of methane over a Ni/Al_2O_3 catalyst in a coaxial dielectric barrier discharge reactor, J. Phys. D. Appl. Phys. 44 (2011) 274007. doi:10.1088/0022-3727/44/27/274007.

[41] G.J.M. Hagelaar, L.C. Pitchford, Solving the Boltzmann equation to obtain electron transport coefficients and rate coefficients for fluid models, Plasma Sources Sci. Technol. 14 (2005) 722–733, https://doi.org/10.1088/0963-0252/14/4/011.

[42] D. Mei, X. Tu, Conversion of CO_2 in a cylindrical dielectric barrier discharge reactor: Effects of plasma processing parameters and reactor design, J. CO2 Util. 19 (2017) 68–78, https://doi.org/10.1016/j.jcou.2017.02.015.

[43] R. Snoeckx, R. Aerts, X. Tu, A. Bogaerts, Plasma-based dry reforming: A computational study ranging from the nanoseconds to seconds time scale, J. Phys. Chem. C. 117 (2013) 4957–4970, https://doi.org/10.1021/jp311912b.

[44] A. Bogaerts, T. Kozák, K. Van Laer, R. Snoeckx, Plasma-based conversion of CO_2: Current status and future challenges, Faraday Discuss. 183 (2015) 217–232, https://doi.org/10.1039/c5fd00053j.

[45] T. Kozák, A. Bogaerts, Splitting of CO_2 by vibrational excitation in non-equilibrium plasmas: A reaction kinetics model, Plasma Sources Sci. Technol. 23 (2014) 045004, https://doi.org/10.1088/0963-0252/23/4/045004.

[46] A. Bogaerts, C. De Bie, R. Snoeckx, T. Kozák, Plasma based CO_2 and CH_4 conversion: A modeling perspective, Plasma Process. Polym. 14 (2017) e1600070, https://doi.org/10.1002/ppap.201600070.

[47] C. De Bie, J. Van Dijk, A. Bogaerts, The dominant pathways for the conversion of methane into oxygenates and syngas in an atmospheric pressure dielectric barrier discharge, J. Phys. Chem. C. 119 (2015) 22331–22350, https://doi.org/10.1021/acs.jpcc.5b06515.

[48] J. Pan, T. Chen, Y. Gao, Y. Liu, S. Zhang, Y. Liu, T. Shao, Numerical modeling and mechanism investigation of nanosecond-pulsed DBD plasma-catalytic CH_4 dry reforming, J. Phys. D. Appl. Phys. 55 (2022) 035202, https://doi.org/10.1088/1361-6463/ac2ad8.

[49] Y. Yi, S. Li, Z. Cui, Y. Hao, Y. Zhang, L.i. Wang, P. Liu, X. Tu, X. Xu, H. Guo, A. Bogaerts, Selective oxidation of CH_4 to CH_3OH through plasma catalysis:

Insights from catalyst characterization and chemical kinetics modelling, Appl. Catal. B Environ. 296 (2021) 120384, https://doi.org/10.1016/j.apcatb.2021.120384.
[50] P. Chawdhury, Y. Wang, D. Ray, S. Mathieu, N.i. Wang, J. Harding, F. Bin, X. Tu, C. h. Subrahmanyam, A promising plasma-catalytic approach towards single-step methane conversion to oxygenates at room temperature, Appl. Catal. B Environ. 284 (2021) 119735, https://doi.org/10.1016/j.apcatb.2020.119735.
[51] L.M. Martini, G. Dilecce, G. Guella, A. Maranzana, G. Tonachini, P. Tosi, Oxidation of CH_4 by CO_2 in a dielectric barrier discharge, Chem. Phys. Lett. 593 (2014) 55–60, https://doi.org/10.1016/j.cplett.2013.12.069.
[52] H.G. Yu, J.T. Muckerman, T.J. Sears, A theoretical study of the potential energy surface for the reaction OH + CO → H + CO_2, Chem. Phys. Lett. 349 (2001) 547–554, https://doi.org/10.1016/S0009-2614(01)01238-6.
[53] H.M. Ogden, T.J. Michael, M.J. Murray, Q. Liu, C. Toro, A.S. Mullin, The effect of CO rotation from shaped pulse polarization on reactions that form C_2, Phys. Chem. Chem. Phys. 21 (2019) 14103–14110, https://doi.org/10.1039/c8cp06917d.
[54] F. Kong, Q.i. Luo, H. Xu, M. Sharifi, D.i. Song, S.L. Chin, Explosive photodissociation of methane induced by ultrafast intense laser, J. Chem. Phys. 125 (2006) 133320, https://doi.org/10.1063/1.2204919.
[55] A. Azarm, H.L. Xu, Y. Kamali, J. Bernhardt, D. Song, A. Xia, Y. Teranishi, S.H. Lin, F. Kong, S.L. Chin, Direct observation of super-excited states in methane created by a femtosecond intense laser field, J. Phys. B At. Mol. Opt. Phys. 41 (2008) 225601, https://doi.org/10.1088/0953-4075/41/22/225601.